

FIFTH INTERNATIONAL CONGRESS ON SOUND AND VIBRATION

DECEMBER 15-18, 1997
ADELAIDE, SOUTH AUSTRALIA

Invited Paper

TRANSIENT WAVE ENVELOPE ELEMENTS FOR UNBOUNDED PROBLEMS

R. J. Astley

Department of Mechanical Engineering, University of Canterbury,
Christchurch, New Zealand.

ABSTRACT

A wave-envelope element numerical scheme is presented for steady and transient unbounded wave problems. The formulation is characterised by the use of conjugated weighting functions which yield frequency-independent mass, stiffness and damping matrices for a discrete frequency-domain model. This can be transformed directly into the time domain and leads to transient equations for exterior nodal pressures which are local. Implicit and semi-explicit methods are used to solve these equations. There are advantages to formulating the proposed elements in spheroidal rather than conventional spherical polar coordinates. Specifically, the size of the conventional finite element mesh which is required in the vicinity of slender or flat radiating objects can be reduced without compromising the completeness of the trial solution in the outer region. A mapped spheroidal formulation is proposed and computed test solutions are presented. An indirect transient solver is also proposed for the solution of the transient discrete equations. This does not require the storage of non-zero or "fill" terms and reduces by a large factor the matrix storage and overall CPU requirements for large three-dimensional transient problems.

1. INTRODUCTION.

The treatment of radiation boundary conditions at the "open" boundaries of unbounded acoustical problems presents a major challenge for computation. The use of discrete node-based or grid-based schemes requires a suitable anechoic termination at the edge of a finite computational region. The more compact and manageable the inner region, the more demanding the numerical treatment that is required on its boundary. This difficulty is circumvented by a variety of Boundary Element (BE) techniques which represent the exterior solution as a surface distribution of source terms. BE schemes are intrinsically non-local in space and result in fully populated coefficient matrices, negating to some extent the economies implicit in using a surface rather than a volume discretisation.

The perception that the BE approach is the most effective numerical option for the computation of unbounded problems has been challenged in recent years by an expanding repertoire of *domain-based* methods. These generally involve finite element (FE) discretisations in an inner region coupled to local or non-local anechoic treatments at a finite boundary. They have higher algebraic dimensionality than comparable BE models but generate more sparsely connected systems of equations. "Infinite elements" have also been applied to such problems (Bettess 1992). The interpolation functions within such elements contain outwardly propagating wave-like factors. Early formulations of this type did not correctly model asymptotic behaviour but subsequent "mapped" formulations are asymptotically correct in the far field. More recently, spheroidal coordinate systems have been used to formulate infinite elements. This permits - in theory at least - a more compact inner discretisation (Burnett 1994). With the exception of the formulation of Olson and Bathe (1987) which is strictly valid only in the limits of high and low frequency, infinite elements have been formulated exclusively in the frequency domain.

Wave envelope elements (Astley 1983, Astley and Eversman 1988) and more recently mapped wave envelope elements (Bettess 1987, Astley et al 1994) employ interpolation functions similar to those of regular infinite elements but use conjugated weighting functions. Although developed primarily for use in the frequency domain, wave envelope elements can readily be applied to the analysis of transient problems (Astley 1996).

In the remainder of this article, a wave-envelope element numerical scheme is presented for the solution of axisymmetric problems. Spheroidal element geometries are used. The formulation is based on a Fourier transformation of a discrete wave envelope model formulated in the frequency domain. The resulting transient equations are local in space and time. The accuracy of the scheme is demonstrated by a comparison of computed and analytic solutions for axisymmetric test cases.

2. THE EXTERIOR ACOUSTIC PROBLEM

The geometry of the problem is shown in figure 1(a). A solution is sought for the exterior sound field generated by the motion of a closed surface S at rest at time $t=0$. The exterior region R is divided into a finite inner region R_i and an unbounded outer region R_o separated by an interface Γ (see figure 1(a)). The acoustic pressure $p(\mathbf{x},t)$ is initially zero at all points. For $t > 0$, $p(\mathbf{x},t)$ is governed by

$$\nabla^2 p = \frac{1}{c^2} \frac{\partial^2 p}{\partial t^2}, \quad \text{in } R \quad (1)$$

$$\text{and } \nabla p \cdot \mathbf{n} = -\rho_0 a_n, \quad \text{on } S \quad (2)$$

where \mathbf{n} is a unit vector normal to S , ρ_0 and c are the mean fluid density and sound speed, and $a_n(\mathbf{x},t)$ is the normal acceleration of S . At large distances from S , the solution satisfies the Sommerfeld radiation condition;

$$r\{\partial p/\partial r + (1/c)\partial p/\partial t\} \rightarrow 0, \quad \text{as } r \rightarrow \infty, \quad (3)$$

where r is a spherical radial coordinate. This is satisfied by the transient initial value solution but must be imposed as a necessary condition for the time-harmonic problem. The transient acoustic pressure $p(\mathbf{x},t)$ and its complex Fourier transform, $\bar{p}(\mathbf{x},\omega)$ are related by the transform pair

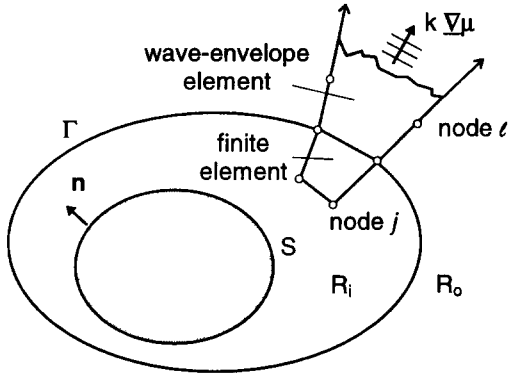


Figure 1(a). Problem geometry.

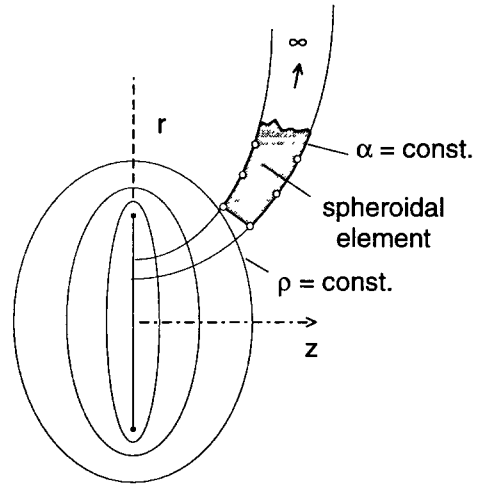


Figure 1(b). Topology of an oblate spheroidal element.

$$\bar{p}(\mathbf{x}, \omega) = \mathcal{F}\{p(\mathbf{x}, t)\} = \int_{-\infty}^{+\infty} p(\mathbf{x}, t) e^{-i\omega t} dt, \quad (4a)$$

$$\text{and } p(\mathbf{x}, t) = \mathcal{F}^{-1}\{\bar{p}(\mathbf{x}, \omega)\} = \frac{1}{2\pi} \int_{-\infty}^{+\infty} \bar{p}(\mathbf{x}, \omega) e^{i\omega t} d\omega. \quad (4b)$$

Equations (1)-(3) then transform to

$$\nabla^2 \bar{p} + k^2 \bar{p} = 0 \quad \text{in } R, \quad (5)$$

$$\nabla \bar{p} \cdot \mathbf{n} = -\rho_a \bar{a}_n \quad \text{on } S, \quad (6)$$

$$\text{and } r^a \{\partial \bar{p} / \partial r + (ik) \bar{p}\} \rightarrow 0, \quad \text{as } r \rightarrow \infty, \quad (7)$$

where $k = \omega/c$ and $\bar{a}_n(\mathbf{x}, \omega)$ is the complex Fourier transform of $a_n(\mathbf{x}, t)$. Alternatively equations (5)-(8) define the steady harmonic problem where $\bar{p}(\mathbf{x}, \omega)$ is the complex pressure amplitude.

3. THE WAVE ENVELOPE FORMULATION.

The wave envelope (WE) formulation is based on a discrete representation of the acoustic pressure amplitude of the form

$$\bar{p}(\mathbf{x}, \omega) = \sum_{j=1}^n \bar{q}_j(\omega) \varphi_j(\mathbf{x}, \omega), \quad (8)$$

where $\varphi_j(\mathbf{x}, \omega)$ ($j=1, \dots, n$) are known basis functions and $\bar{q}_j(\omega)$ ($j=1, \dots, n$) are unknown coefficients. Equation (9) is valid over the entire exterior region R . Application of a Galerkin procedure with weighting functions $W_j(\mathbf{x}, \omega)$ ($j=1, 2, \dots, n$) then yields a system of linear equations;

$$[\mathbf{A}(\omega)] \bar{\mathbf{q}} = \bar{\mathbf{f}} \quad (9)$$

where $\bar{\mathbf{q}}$ is the vector whose components are the trial coefficients $q_i(\omega)$ ($i=1, \dots, n$), \mathbf{A} is an $n \times n$ coefficient matrix and $\bar{\mathbf{f}}$ an $n \times 1$ forcing vector. \mathbf{A} and $\bar{\mathbf{f}}$ have components;

$$A_{ij} = \int_R \left\{ \nabla W_i \cdot \nabla \phi_j - k^2 W_i \phi_j \right\} dR, \quad \text{and} \quad \bar{f}_i = \int_S \rho_a W_i \bar{a}_n dS. \quad (10a,b)$$

The weight and basis functions W_i and ϕ_j are chosen so that the above integrals are finite. They are defined as follows:

(a) In the inner region R_i , a regular FE model is used. i.e

$$W_j(\mathbf{x}, \omega) = \phi_j(\mathbf{x}) = N_j(\mathbf{x}), \quad (11)$$

where $N_j(\mathbf{x})$, is the global finite element shape function associated with node j (see figure 1(a)). The corresponding coefficients $\bar{q}_j(\omega)$ are nodal values of the pressure amplitude $\bar{p}(\mathbf{x}, \omega)$.

(b) In the outer region, R_o , the basis functions $\phi_l(\mathbf{x}, \omega)$ corresponding to node l say (see figure 1(a)) are given by

$$\phi_l(\mathbf{x}, \omega) = P_l(\mathbf{x}) e^{-i k \mu(\mathbf{x})} \quad (12)$$

where k is the scalar wave number ($=\omega/c$) and where the phase function $\mu(\mathbf{x})$ is chosen so that $\nabla \mu$ is aligned with the (estimated) direction of wave propagation. In the case of an axisymmetric spheroidally formulated element, $\nabla \mu$ lies along a local radial direction in a prolate or oblate spheroidal coordinate system. The orientation of an oblate spheroidal element with respect to spheroidal coordinates ρ and α is indicated in figure 1(b). The interpolation function $P_l(\mathbf{x})$ then defines an “envelope” of waves of vector wavenumber $k \nabla \mu$. In the case of a spheroidal element the dependence of $P_l(\mathbf{x})$ on a spheroidal radius ρ is a polynomial in $(1/\rho)^2$ of order $m+1$ where m is the number of nodes along the infinite side of the element. The phase function $\mu(\mathbf{x})$ is proportional to ρ . A mapping is used to define these functions (Astley 1997). The weighting functions within the element are then defined as

$$W_l(\mathbf{x}, \omega) = D(\mathbf{x}) [\phi_l(\mathbf{x}, \omega)]^* = D(\mathbf{x}) P_l(\mathbf{x}) e^{+i k \mu(\mathbf{x})}, \quad (13)$$

where $[]^*$ denotes a complex conjugate and $D(\mathbf{x})$ is a geometric factor which behaves as $(1/\rho^2)$ and takes the value of unity at the interface between the wave envelope region and the FE mesh. The presence of the conjugate term in the weighting functions greatly simplifies the integrals of equations (10) and permits a simple transformation to the time domain.

Upon substitution of expressions (11-13) into integral (10a), it is not difficult to show that the coefficient matrix $A(\omega)$ can be written in terms of frequency-independent sub-matrices \mathbf{K} , \mathbf{C} , and \mathbf{M} . Equation (9) then becomes

$$[\mathbf{K} + i\omega\mathbf{C} - \omega^2\mathbf{M}]\bar{\mathbf{q}} = \bar{\mathbf{f}}, \quad (14)$$

which can be transformed directly into the time domain to give

$$\mathbf{K}\mathbf{q} + \mathbf{C}\dot{\mathbf{q}} + \mathbf{M}\ddot{\mathbf{q}} = \mathbf{f}(t), \quad (15)$$

where $q_i(t) = \mathcal{F}^{-1}\{\bar{q}_i(\omega)\}$, and $f_i(t) = \mathcal{F}^{-1}\{\bar{f}_i(\omega)\}$. The components $f_i(t)$ can moreover be assembled directly in the time domain, being given by

$$f_i = \int_S \rho N_i a_n(\mathbf{x}, t) dS. \quad (16)$$

The components of the transient solution vector $\mathbf{q}(t)$ within the inner region correspond to instantaneous nodal values of acoustic pressure. In the WE region, they represent

instantaneous nodal pressures at a delayed time equal to the time required for a disturbance to propagate from the edge of the inner mesh (Astley 1996).

4. SOLUTION IN THE FREQUENCY DOMAIN.

A complex L-U solver is used to solve equation (14). A “skyline” storage algorithm takes advantage of the sparse structure within the coefficient matrix. In calculating a frequency response over a range of frequencies, the stiffness, mass and damping matrices, \mathbf{K} , \mathbf{C} , and \mathbf{M} are assembled once only.

5. DIRECT SOLUTION OF THE TRANSIENT EQUATIONS.

In the transient case, a direct time-integration scheme is used to solve equation (15). In the absence of any clear strategy for lumping the mass and damping matrices - which would make an explicit scheme attractive - the implicit “average acceleration” (Newmark: $\beta = 1/4$, $\gamma = 1/2$) method is used. The algorithm at each time step is given by;

$$\mathbf{E}\mathbf{q}_{t+\delta t} = \mathbf{f}_{t+\delta t} + \mathbf{G}\mathbf{q}_t + \mathbf{H}\dot{\mathbf{q}}_t + \mathbf{J}\ddot{\mathbf{q}}_t \quad (17a)$$

$$\ddot{\mathbf{q}}_{t+\delta t} = (4/\delta t^2)(\mathbf{q}_{t+\delta t} - \mathbf{q}_t) - (4/\delta t)\dot{\mathbf{q}}_t - \ddot{\mathbf{q}}_t \quad (17b)$$

$$\dot{\mathbf{q}}_{t+\delta t} = \dot{\mathbf{q}}_t + (\delta t/2)(\ddot{\mathbf{q}}_t + \ddot{\mathbf{q}}_{t+\delta t}) \quad (17c)$$

where the subscripts “ t ” and “ $t+\delta t$ ” denote values of \mathbf{q} at successive time steps. The matrices \mathbf{E} , \mathbf{G} , \mathbf{H} and \mathbf{J} are given by

$$\mathbf{E} = \mathbf{K} + (2/\alpha)\mathbf{C} + (4/\alpha^2)\mathbf{M}, \quad \mathbf{G} = (2/\alpha)\mathbf{C} + (4/\alpha^2)\mathbf{M}, \quad \mathbf{H} = \mathbf{C} + (4/\alpha)\mathbf{M}, \quad \text{and} \quad \mathbf{J} = \mathbf{M}. \quad (17d)$$

An L-U solver is used, the decomposition being performed once only at the first time step. This scheme is known to be unconditionally stable for symmetric problems but there is no assurance that this is the case in the current instance given that \mathbf{K} and \mathbf{C} are not symmetric. Stable solutions have been obtained however in all of the test solutions to date.

6. ITERATIVE SOLUTION OF THE TRANSIENT EQUATIONS.

The calculation and storage of “fill terms”, generated during the decomposition of \mathbf{E} , forms a significant computational overhead in the implicit scheme. This can be avoided by splitting the diagonal and non-diagonal terms of \mathbf{E} and solving equation (17a) iteratively. Equation (17a) is replaced by

$$\mathbf{q}_{t+\delta t}^{n+1} = \mathbf{D}^{-1}[\mathbf{f}_{t+\delta t} + \mathbf{G}\mathbf{q}_t + \mathbf{H}\dot{\mathbf{q}}_t + \mathbf{J}\ddot{\mathbf{q}}_t - \mathbf{L}\mathbf{q}_{t+\delta t}^n - \mathbf{U}\mathbf{q}_{t+\delta t}^{n+1}] \quad (18)$$

where $\mathbf{q}_{t+\delta t}^n$ denotes the value of the solution vector at time $t+\delta t$ after n iterations have been performed. Here \mathbf{D} , \mathbf{L} , and \mathbf{U} are diagonal, lower and upper matrices where; $\mathbf{E} = \mathbf{D} + \mathbf{L} + \mathbf{U}$. Convergence is assumed when

$$\left| \mathbf{q}_{t+\delta t}^{n+1} - \mathbf{q}_{t+\delta t}^n \right| / \left| \mathbf{q}_{t+\delta t}^n \right| \leq \epsilon \quad (19)$$

where ϵ is a prescribed value. Convergence will be shown to be rapid provided that the time step is sufficiently small.

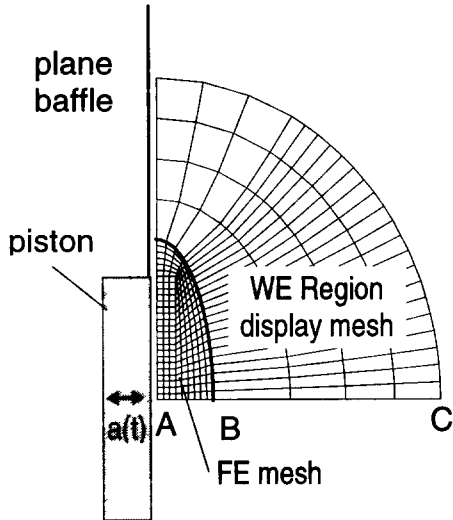


Figure 2. Test case, FE/WE mesh

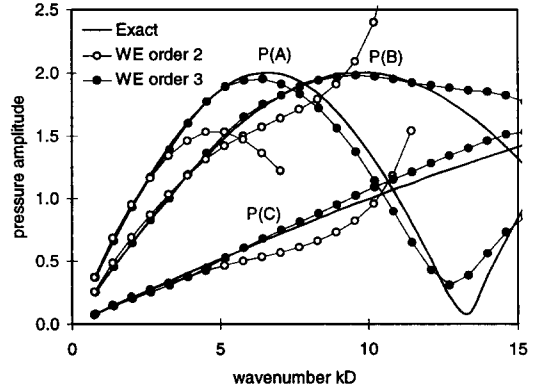


Figure 3. Test case, steady response,

7. RESULTS.

The performance of the method is demonstrated by the presentation of computed results for the sound field generated by a cylindrical piston in a plane baffle. Computed solutions are obtained for the FE/WE mesh shown in figure 2. The WE elements are based on an oblate spheroidal formulation. The problem is axially symmetric about the line ABC . In the steady case the piston undergoes time harmonic excitation, $a(t) = a_0 e^{i\omega t}$. In the unsteady case, it experiences a single pulse: $a(t) = 0$, $t < 0$, $a(t) = a_0 \sin \omega t$, $0 < t < \pi/\omega$, and $a(t) = 0$, $t > \pi/\omega$.

7.1 Steady solutions, the effect of element order.

The effect of element order on the accuracy of the computed solution is demonstrated in figure 3 which shows a comparison of computed and analytic frequency responses at the points A , B and C . These results are obtained by solving equation (14). The non-dimensional acoustic pressure amplitude $|\bar{p} \omega / \rho_0 c a_0|$ is plotted against non-dimensional wavenumber kD where D is the diameter of the piston. Results are presented for WE elements of radial orders 2 and 3. At the upper end of the frequency range - ie at $kD = 15.0$ - the spatial resolution of the inner FE mesh is marginal in terms of its ability to represent a wave-like solution. Some deterioration in accuracy is therefore anticipated as frequency increases. In the current instance however accuracy is clearly limited by the radial order of the WE mesh rather than by resolution of the conventional inner region. The same effect is apparent in other test cases for which solutions have been computed using both prolate and oblate spheroidal elements. In some respects this acts to limit the effectiveness of the spheroidal formulation in decreasing the extent of the FE region in that the reduction in the number of nodes within the FE region is generally offset by an increase in radial resolution in outer region to maintain accuracy.

7.2 Transient solutions, the effect of step size.

Exact and computed transient solutions for the impulsively excited piston are shown in figures 4(a) and (b). Pressure histories are plotted against dimensionless time $T (=tc/D)$ at points A

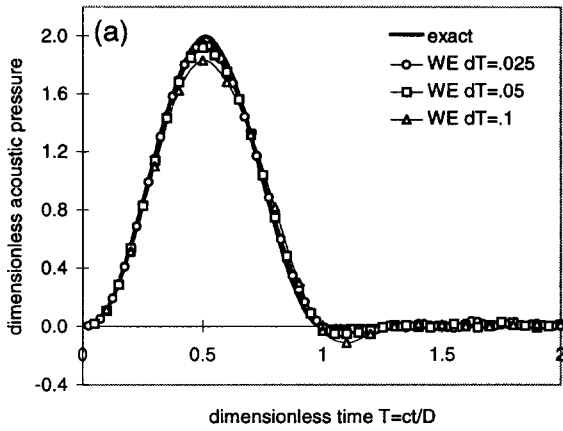


Figure 4(a) Transient response at A.

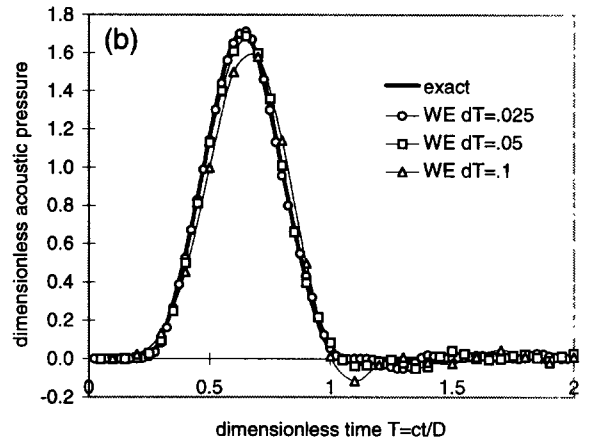


Figure 4(b) Transient response at B.

and B . The piston acceleration takes the form of a single half-wave pulse of duration 0.5 units of dimensionless time. WE elements of order 3 are used. Results are shown for time steps: $\delta T=.025$, $\delta T=.05$ and $\delta T=.10$. The smallest of these ($\delta T=.025$) is equal to the time which elapses as a disturbance propagates between adjacent nodes on the face of the piston. All solutions are stable but those obtained by using the largest time step ($\delta T=.10$) are marginal in terms of accuracy. This is to be anticipated given that this corresponds to approximately one fifth of the duration of the pulse. These results do not constitute proof that the average acceleration scheme is unconditionally stable when applied to other problems but do lend weight to this supposition.

7.3 The performance of the iterative solver.

The performance of the iterative scheme is illustrated in figures 5(a) and (b). The data presented in these figures are obtained by applying the iterative scheme of equation (18) to the solution of the transient test problem. The pressure histories re-computed in this way are indistinguishable to the scale shown from those shown in figure provided that $\epsilon < 10^{-3}$. The rate of convergence of the iterative scheme is illustrated in figure 5 for various settings. In all cases, the iterative solver runs for 100 time steps and an iteration count is performed at each step. The results are presented in bar-chart format as the percentage of solution steps for which convergence was achieved after a given number of iterations. The effect of varying the parameter ϵ is shown in figure (a), that of varying the step size is shown in figure (b). The results of figure (5a) are obtained by fixing the time step at $\delta T=.025$ and varying ϵ in the range $10^{-3} - 10^{-6}$. As ϵ decreases the convergence criterion becomes more stringent and more iterations are required. The numbers are modest however, with 5-10 iterations generally giving solutions which are indistinguishable for all practical purposes from those obtained from the implicit scheme.

The effect of step size is illustrated in figure 5(b). Here the convergence parameter ϵ is fixed at 10^{-3} and the step size is varied from 0.025 to 0.10. The deterioration of the rate of convergence as the time step increases is to be anticipated given that the number of the surrounding nodes which participate in the solution increases once δT exceeds the time taken for a disturbance to traverse one element (in this case $\delta T=.025$).

Further results - not presented here - indicate that model size does not significantly affect the convergence of the scheme

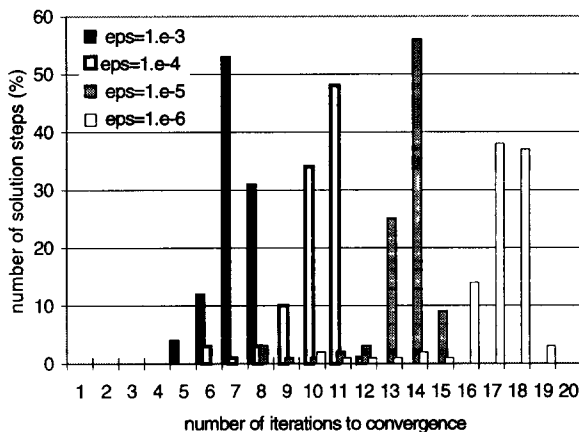


Figure 5(a). Convergence of the iterative scheme, the effect of the parameter ϵ .

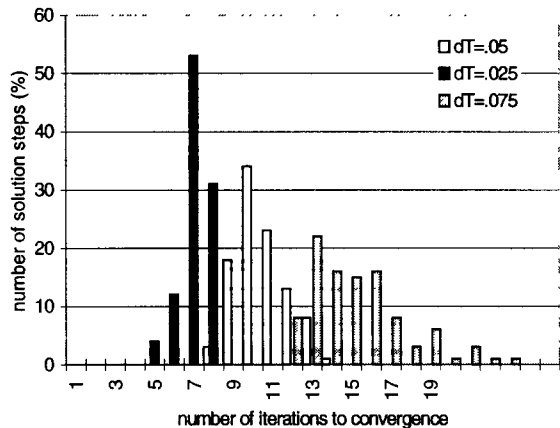


Figure 5(b). Convergence of the iterative scheme, the effect of step size.

8. CONCLUSIONS.

- An implicit time integration scheme has been implemented with a transient wave envelope formulation and has been shown to give accurate and (apparently) stable solutions
- The selection of step size is governed by considerations of accuracy in resolving the temporal variation rather than by time-scales associated with the mesh.
- An iterative scheme which does not require a matrix inversion has been demonstrated and has been shown to converge rapidly provided that the time step is smaller than a characteristic time-scale associated with the mesh.

REFERENCES

- Astley, R J 1983 "Wave envelope and infinite elements for acoustic radiation" *Int. J. Num. Meth. Fluids* **3**, 507-526.
- Astley, R J and Eversman, W , 1988 "Wave envelope elements for acoustical radiation in inhomogeneous media", *Comp. and Struct.* **30**, 801-810 .
- Astley, R. J , Macaulay G. J. and Coyette, J. P, 1994 "Mapped wave envelope elements for acoustic radiation and scattering", *J. Sound Vib.* **170**, 97-118.
- Astley, R. J. 1996 "Transient wave envelope elements for wave problems", *J. Sound Vib.* **192**, 245-261
- Astley, R J, in publication, " Mapped Spheroidal Wave-Envelope Elements for Unbounded Wave Problems" *Int. J. Num. Meth. Engng.*
- Bettess, P., 1987, "A simple wave envelope example". *Comm.Appl.Num. Meth.* **3**, 77-80.
- Bettess, P, 1992, *Infinite Elements*. Penshaw Press, Sunderland.
- Burnett, D S, 1994, "A three dimensional acoustic infinite element based on a prolate spheroidal multipole expansion", *J. Acoust. Soc. Am.* **96**, 2798-2816 .
- Olson, L G and Bathe, K J, 1985, "An Infinite Element for the Analysis of Fluid-Structure Interaction", *Eng. Comput.* **2**, 319-329.